Coulomb effects on edge scattering in elastic nuclear collisions

R. da Silveira
Groupe de Physique Théorique, Institut de Physique Nucléaire, F-91406 Orsay Cedex, France

Ch. Leclercq-Willain
Physique Nucléaire Théorique et Mathématique, Code Postal 229, Universite Libre de Bruxelles, B-1050 Bruxelles, Belgium

(Received 15 February 2011; published 11 April 2011)

We present a qualitative analysis of the effects of the Coulomb force on the edge scattering produced in elastic nuclear collisions occurring under strong absorption conditions. This analysis is illustrated with several examples of nucleus-nucleus and antiproton-nucleus elastic scattering.

DOI: 10.1103/PhysRevC.83.044603 PACS number(s): 25.70.−z, 25.60.Bx, 25.43.+t, 24.10.Ht

To provide some physical insight into nuclear collision mechanisms such as edge and shadow scattering, it is convenient to write the elastic amplitude in the form

$$f(\theta) = f_c(\theta) + f_n(\theta), \tag{1}$$

where $f_c(\theta)$ is the Coulomb amplitude. The amplitude $f_n(\theta)$ is often called the "nuclear amplitude" although it retains, of course, a Coulomb dependence. We are concerned with nuclear collisions occurring under strong absorption conditions. This means that all partial waves up to a grazing angular momentum $l = l_g$ are absorbed, while all higher ones undergo Coulomb scattering [1–3].

Under these conditions, the amplitude $f_n(\theta)$ has a specific physical interpretation according to the strength of the Coulomb effects. These effects are measured by the Sommerfeld parameter $\eta = \frac{Z_1 Z_2 e^2}{\hbar v}$. For $|\eta| \gg 1$, $f_n(\theta)$ is interpreted as the amplitude of the waves scattered by the edge or the surface of the target. In a semiclassical description, these waves are associated with the trajectories deviated through angles close to the grazing angle $\theta_g \cong \frac{2|\eta|}{l_g}$. These waves produce the familiar angular dependence [4,5]

$$|f_n(\theta)|^2 \propto J_0^2(l_g\theta). \tag{2}$$

According to whether the description of the collision is quantal or semiclassical, this $J_0^2(l_g\theta)$ behavior is called edge or glory scattering, respectively.

For $|\eta| \lesssim 1$, the Coulomb contribution becomes negligible outside the nearest forward direction, and the strong absorption regime leads to a shadow effect. The well-known Fraunhöfer diffraction angular dependence [1–3]

$$|f(\theta)|^2 \cong |f_n(\theta)|^2 \propto [J_1(l_g\theta)/l_g\theta]^2 \tag{3}$$

originates from this shadow effect. So, when going from large to small Coulomb effects, $|f_n(\theta)|^2$ changes from a glory-like pattern to a Fraunhöfer-like one.

The purpose of this note is to investigate how this change takes place and mostly how the signature of edge scattering as given by expression (2) remains. To this end we analyze several examples of nucleus-nucleus and antiproton-nucleus elastic collisions covering a range of η values going from $|\eta| = 8.18$ to $|\eta| = 0.23$.

For large Coulomb effects ($|\eta| \gg 1$), there are several model-independent methods [6–8] allowing extraction of $|f_n(\theta)|$ from the measured scattering cross section, providing sufficiently accurate experimental data are available at very small angles. This is the case for the two examples: $^{16}O + ^{28}Si$, $\eta = 8.18$ and $^{12}C + ^{28}Si$, $\eta = 5.7$ [9].

From the analysis of these data, we are able to identify clearly for $|f_n(\theta)|$ the pronounced rise as well as the first extrema of the J_0 Bessel function. One obtains [7,8]

$$|f_n(\theta)|^2 \approx |f_n(0)|^2\, J_0^2(l_g\theta), \quad \theta \ll \theta_g, \tag{4}$$

with $|f_n(0)| = 43$ fm, $l_g = 32$ for ^{16}O on ^{28}Si and $|f_n(0)| = 22$ fm, $l_g = 28$ for ^{12}C on ^{28}Si.

Let us now compare this result with the prediction of an optical model calculation which fits the measured scattering cross section $d\sigma/d\Omega = |f_c + f_n|^2$. All the numerical calculations utilize Woods-Saxon form factors in both the real and the imaginary parts of the optical potential. For $^{12}C + ^{28}Si$ at 65 MeV and $^{16}O + ^{28}Si$ at 75 MeV, the parameters [10] are given in Table I.

The comparison between expression (4) using the parameters deduced from the data and the optical model prediction is displayed in Figs. 1 and 2. The results are plotted versus $x = l_g\theta$,which allows better identification of the oscillatory regime as given by expressions (2) or (3). The points are the measured values of $d\sigma/d\Omega$ (relative to the Rutherford cross section $d\sigma_R/d\Omega$) and the broken line is the result of the optical model fit.The solid and dot-dashed lines are, respectively, the calculated expressions $(|f_n(x/l_g)|^2/|f_n(0)|^2)$ and $J_0^2(x)$. As one can see in Figs. 1 and 2, the optical model results show a glory-like behavior over a range of x extending to $x \cong 2|\eta|$, i.e., $\theta \cong \theta_g$.

For small Coulomb effects ($|\eta| \lesssim 1$), the method used above to obtain $|f_n(\theta)|$ from the experimental data fails. So let us consider the same colliding partners but with small η values: $^{16}O + ^{28}Si$, $\eta = 1.82$, $l_g = 144$ [11] and $^{12}C + ^{28}Si$, $\eta = 3.35$, $l_g = 51$ [12]. The grazing angular momentum is determined, as usual, by the relation $l_g \cong \frac{2\pi}{\Delta\theta}$ where $\Delta\theta$ is the angular spacing between successive maxima (or minima) of the measured ratio $d\sigma/d\sigma_R$. Figures 3 and 4 show the experimental data $d\sigma/d\sigma_R$ (points) for ^{16}O and ^{12}C, respectively, plotted versus $x = l_g\theta$. In each figure, the broken line is the result of the optical model fit with the potential given in Table I for each collision. The oscillations of $d\sigma/d\sigma_R$ are clearly reminiscent of a Fraunhöfer

TABLE I. Selected elastic scattering data and the optical Woods-Saxon potential parameters used in the calculation.

Collision	Energy (MeV)	η	V_0 (MeV)	r_v (fm)	a_v (fm)	W_0 (MeV)	r_w (fm)	a_w (fm)
^{12}C+^{28}Si	65	5.75	10.0	1.38	0.484	24.67	1.23	0.413
	186.4	3.35	10.0	1.32	0.617	30.3	1.16	0.609
^{16}O+^{28}Si	75	8.18	10.0	1.38	0.456	41.84	1.13	0.575
	1503	1.82	100.0	0.892	0.905	50.5	0.992	0.780
$\overline{p}$+^{208}Pb	48.6	−1.85	0.0	–	–	22.0	1.38	0.5
$\overline{p}$+^{40}Ca	179.8	−0.23	40.5	1.10	0.63	111.0	1.10	0.63

diffraction pattern, easily identified by drawing the successive minima of expression (3)(vertical dashed lines).

To go further we will invoke by optical analogy an extension of the Babinet's principle [13] which can be formulated as follows: the Fraunhöfer diffraction pattern produced by an opaque screen and the one produced by a narrow slit having the same shape of its edge, oscillate 180° out of phase or in quadrature, i.e., the maxima of one pattern coincide with the minima of the other and vice versa. By considering the asymptotic forms of the Bessel functions $J_0(l_g\theta)$ and $J_1(l_g\theta)$, $\theta \gg 1/l_g$, i.e.,

$$J_n(l_g\theta) \approx \sqrt{\frac{2\pi}{l_g\theta}} \cos\left(l_g\theta - n\frac{\pi}{2} - \frac{\pi}{4}\right) \quad (n = 0, 1), \quad (5)$$

one can see that edge and Frauhöfer scattering as given by expressions (2) and (3), respectively, satisfy this phase rule.

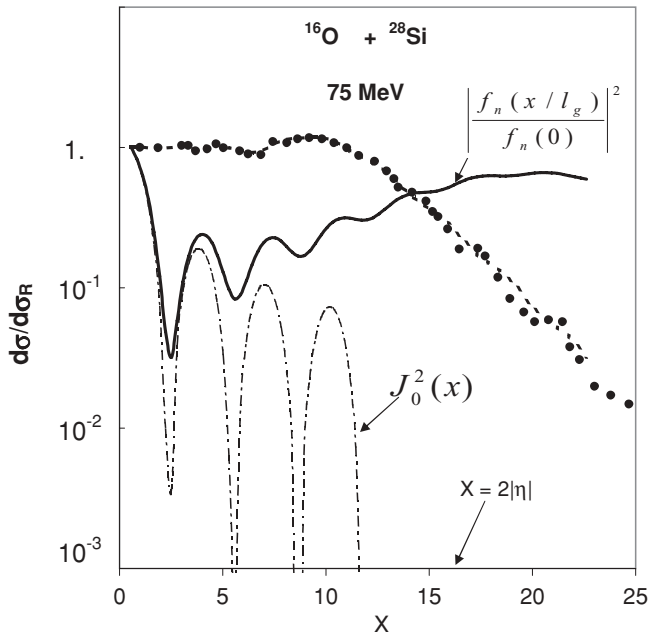

FIG. 1. Angular distribution of elastic scattering of ^{16}O on ^{28}Si at $E = 75$ MeV ($\eta = 8.18$). The experimental data $d\sigma/d\sigma_R$ (points) [9], the optical model fit (broken line), the calculated expression $(|f_n(x/l_g)/f_n(0)|^2)$ (solid line), and $J_0(x)^2$ (dot-dashed line) are drawn.

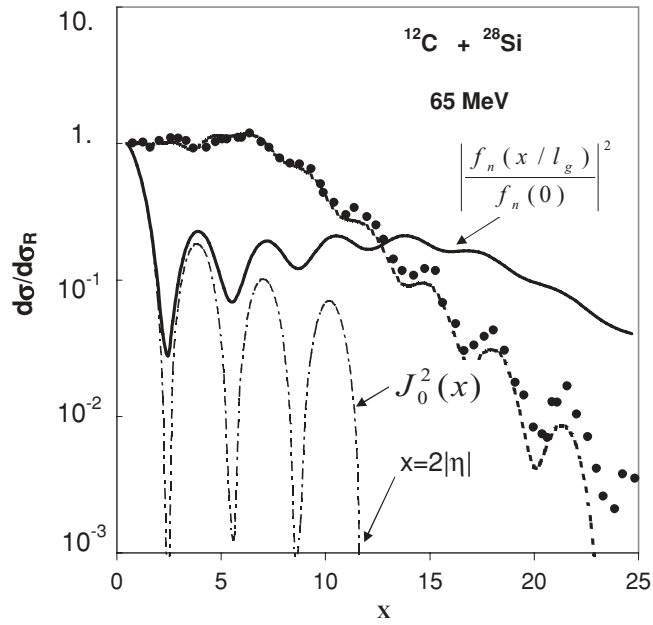

FIG. 2. Same as Fig. 1, but for the elastic scattering of ^{12}C on ^{28}Si at $E = 65$ MeV ($\eta = 5.7$). Experimental data are from Ref. [9].

In Figs. 3 and 4, we now compare the oscillations of the calculated curve $|f_n(x/l_g)|^2$ (solid line) with those of the measured scattering cross section $d\sigma/d\sigma_R$ (points). As seen in both figures, the phase rule is well satisfied for $\theta \lesssim \theta_g$ ($x \lesssim 2|\eta|$). This shows that $|f_n|^2$ still retains a $J_0^2(x)$-like behavior, the fingerprint of edge scattering.

Let us consider now two examples taken from antiproton-nucleus collisions. The antiprotons are strongly absorbed by nuclei and are also good candidates to exhibit edge scattering effects. These examples are [14] $\overline{p}$+^{208}Pb at $E = 48.6$ MeV, $\eta = -1.85$, and $l_g = 14$ and $\overline{p}$+^{40}Ca at $E = 179.8$ MeV, $\eta = -0.23$, and $l_g = 15$. The parameters of the optical potentials are given in Table I. Figure 5 shows the experimental data for $\overline{p}$+^{208}Pb (points), the optical model fit (broken line), and $|f_n(x/l_g)|^2$ (solid line).

The value of η for $\overline{p}$+^{208}Pb ($|\eta| = 1.85$) is very close to that for ^{16}O + ^{28}Si ($\eta = 1.82$), and therefore it is not surprising that Figs. 3 and 5 are qualitatively very similar. The results for $\overline{p}$+^{40}Ca are shown in Fig. 6.

One immediately remarks that the signature of the edge scattering is no longer present and that the curve of $|f_n|^2$ behaves now as a Fraunhöfer diffraction pattern in the whole angular range, in agreement with expression (3).

These results call for the following concluding remarks: what is the condition to observe the "180° out-of-phase rule" between the oscillations of $|f_n(\theta)|^2$ and those of $|f(\theta)|^2$. As earlier noted, edge scattering takes place in the angular domain $\theta \lesssim \theta_g$ ($x \lesssim 2\,|\eta|$), and on the other hand, both the first maximum of $J_0(x)^2$ and the first minimum of $(J_1(x)/x)^2$ occur for x very close to 3.8 (see Figs. 3 and 5). So the observation of the phase rule requires $2|\eta| \gtrsim 3.8$, i.e., $|\eta| \gtrsim 1$. This condition is still well satisfied for ^{16}O + ^{28}Si ($\eta = 1.82$) and $\overline{p}$+^{208}Pb ($|\eta| = 1.85$), but it is largely violated for $\overline{p}$+^{40}Ca ($|\eta| = 0.23$); therefore it is not surprising that the fingerprint of edge scattering is missing in this case.

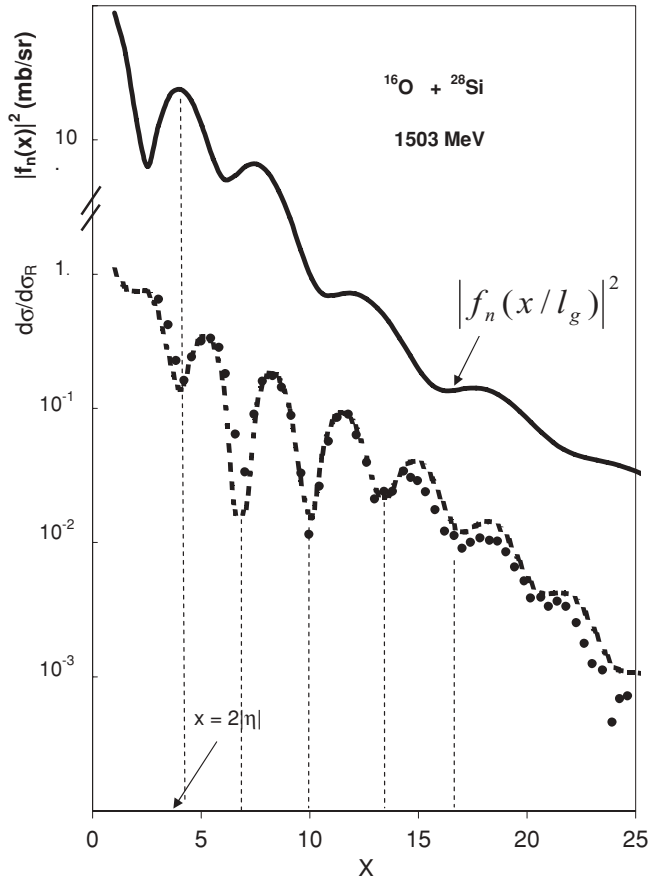

FIG. 3. Angular distribution of elastic scattering of ^{16}O on ^{28}Si at $E = 1503$ MeV ($\eta = 1.82$). The experimental data $d\sigma/d\sigma_R$ (points) [11], the optical model fit (broken line), and the calculated $|f_n(x/l_g)|^2$ mb/Sr (solid line) are drawn. The vertical dashed lines indicate the successive minima of $J_1(x)^2$.

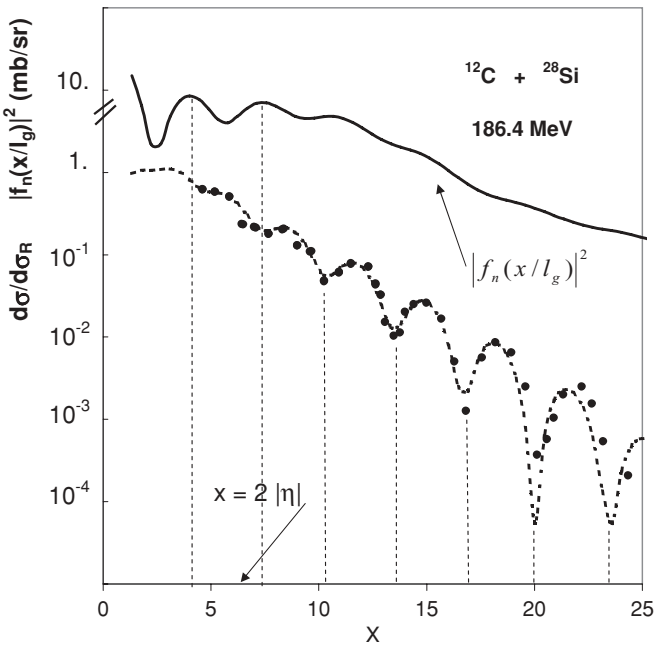

FIG. 4. Same as Fig. 3, but for the elastic scattering of ^{12}C on ^{28}Si at $E = 186.4$ MeV ($\eta = 3.35$). Experimental data are from Ref. [12].

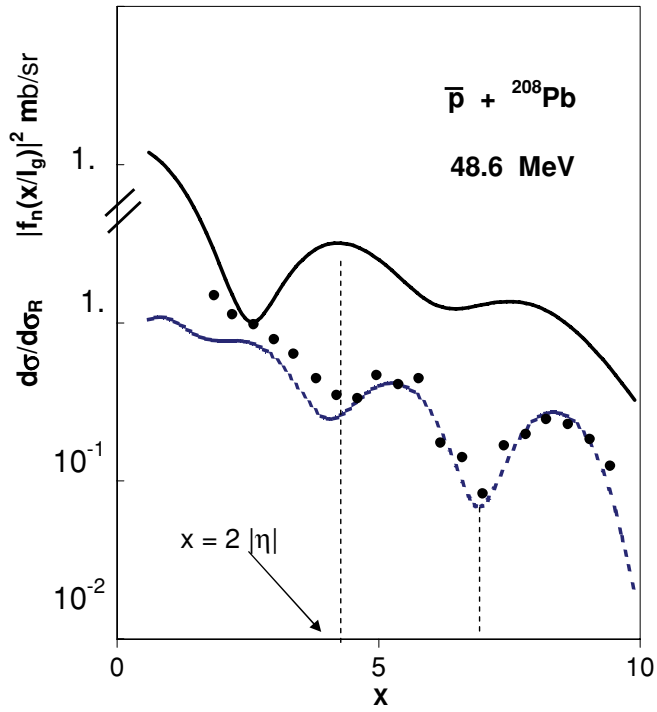

FIG. 5. (Color online) Same as Fig. 3, but for the elastic scattering of $\overline{p}$+^{208}Pb at $E = 48.6$ MeV ($\eta = -1.85$). Experimental data are from Ref. [14].

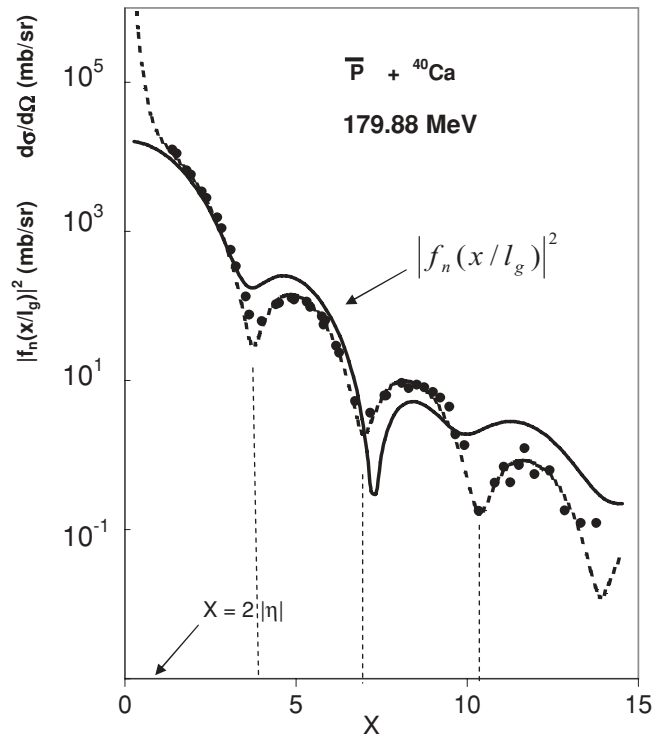

FIG. 6. Angular distribution of elastic scattering of $\overline{p}$+^{40}Ca at $E = 179.8$ MeV ($\eta = -0.23$). The experimental data $d\sigma/d\Omega$ mb/Sr (points) [14], the optical model fit (broken line), the calculated $|f_n(x/l_g)|^2$ mb/Sr (solid line) are drawn. The vertical dashed lines indicate the successive minima of $J_1(x)^2$.

[1] D. M. Brink, *Semiclassical Methods in Nucleus-Nucleus Scattering* (Cambridge University, New York, 1985).
[2] J. S. Blair, *Nuclear Structure Physics*, Lectures in Theoretical Physics, edited by P. D. Kunz, D. A. Lind, and W. E. Britten, Vol. VIII C (University of Colorado, Boulder, 1966).
[3] R. D. Amado, *Advances in Nuclear Physics*, edited by J. W. Negele and E. W. Vogt, Vol. 15 (Plenum, New York, 1985).
[4] K. W. Ford and J. A. Wheeler, Ann. Phys. (NY) **7**, 259 (1959).
[5] H. M. Nussenzveig, *Diffraction Effects in Semiclassical Scattering* (Cambridge University, New York, 1992).
[6] J. Barette and N. Alamanos, Nucl. Phys. A **441**, 733 (1985).
[7] R. da Silveira, A. Boukour, and Ch. Leclercq-Willain, Eur. Phys. J. A **7**, 503 (2000).
[8] R. da Silveira and Ch. Leclercq-Willain, Phys. Rev. C **70**, 44604 (2004).
[9] T. Yamaya *et al.*, Phys. Lett. B **417**, 7 (1998).
[10] T. Yamaya, O. Satoh, S. M. Morita, K. Kotajima, K. Hasegawa, T. Shinozuka, and M. Fujioka, Phys. Rev. C **37**, 2585 (1988).
[11] P. Roussel, N. Alamanos, F. Auger, J. Barrette, B. Berthier, B. Fernandez, L. Papineau, H. Doubre, and W. Mittig, Phys. Rev. Lett. **54**, 1779 (1985).
[12] R. M. DeVries, D. A. Goldberg, J. W. Watson, M. S. Zisman, and J. G. Cramer, Phys. Rev. Lett. **39**, 450 (1977).
[13] R. da Silveira, J. Mod. Opt. **38**, 1349 (1991); Phys. Lett. B **264**, 248 (1991).
[14] S. Janouin *et al.*, Nucl. Phys. A **451**, 541 (1986).